ISSN (Online) 2456 -1304

International Journal of Science, Engineering and Management (IJSEM)

Vol 10, Issue 3, March 2023

Removal Alizarin Red S Using a Modified Magnetic Nanoporous MCM-41 Based Dispersive Micro-Solid-Phase and Response Surface Optimization

[1] Esmail Khaledyan, [2] Soheila Jafari, [3] Bahram Abdollahzadehteimourlouei*, [4] Ali Abbasi Jahanabad, [5] Mehdi Kiani

[1] Department of Pharmacy, Komar University of Science and Technology, Sulaimaniyah, Iraq
[2] Department of Chemical Engineering, Faculty of Engineering, South Tehran Branch, Islamic Azad University, Tehran, Iran
[3] Department of Polymer Chemistry, Faculty of Science, University of Zanjan, Zanjan, Iran
[4] Department of Electrical Engineering, Faculty of Engineering, Azad University of Naein, Iran
[5] Department of Mechanical Engineering , College of Engineering, University of Tehran, Tehran, Iran
Corresponding Author Email: [1] appleiddeveloper47@gmail.com, [2]soheyla.jafari90@gmail.com, [3] abdollahzadebahram@alumni.znu.ac.ir, [4] artkimia99@gmail.com, [5] mehdi.kiany@gmail.com

Abstract*— In this research, a hydrothermally synthesized core-shell structured magnetic mesoporous nanocomposite was modified by 3-aminopropyltriothoxysilane (APTES) as an amine function on the surface nanocomposite and used to remove Alizarin Red S as an anionic dye from aqueous. SEM, FT-IR, XRD, and TEM were used to characterize this nanocomposite. The main parameters that were effective in removing synthesis dye, such as vortex, time, amount of adsorbent, and dye concentration were enhanced using Central Composite Design (CCD) under Response Surface Methodology (RSM). For ARS, 224.21 mg g^{-1} of maximum sorption capacity was found. The equilibrium data fitted to isotherm models revealed that the Langmuir model had the highest R^2 value of 0.9895. Several kinetics models were examined for the optimum model after it was demonstrated that a monolayer of dye forms on the surface of an adsorbent. The findings suggested that the best model for the adsorption rate had an R^2 of 0.9909.

Keywords: Alizarin Red S, Central Composite Design, Dye removal, Langmuir model.

I. INTRODUCTION

One of the challenges in this century is the pollution of water caused by wastewater discharged from businesses like paint, textile, fast fashion, food, cosmetics, plastic, paper, and pharmaceutical [1,2]. Pollution of water resources is posing problems for many biological, environmental, and aquatic species [1, 2]. Anthraquinone-based structure dyes are more stable in the environment and have a lower biodegradability [3-5]. Adsorption has received attention from scientists and engineers as one of many physicochemical methods for treating wastewater since it is inexpensive, reusable, and environmentally friendly, plus the experimental procedure is simple [8-13]. The ability of an adsorbent to extract chemical materials from water is dependent on its high capacity, reusability, and low cost. Magnetic nanoparticles (MNPs) have distinct qualities such as a large surface area, ease and speed of collection from solution, and low diffusion resistance [14-16].

These MNPs require surface alteration and the ensuing core-shell structure. Because of its non-toxicity, and good aggregation, the Silica alteration as the surface shell on particles magnetic as the core has been used [17, 18]. The benefits of this alteration stable MNPs in various chemical mediums that are easily functionalized. Mesoporous surfaces feature more silanol groups that react with alkoxysilane to generate Si-O linkages, whereas terminal function groups can react with APTES [19]. The usage of MNPs-mesoporous modified with APTES as an adsorbent for dye removal has not been applied recently. In this investigation, we used Alizarin Red S, an anionic dye with the structure illustrated in Fig.1. Alizarin Red S was discharged from textile effluent after being used to colour wool and cotton textiles, woven fabrics, rubber, and polymers [20, 21]. This anthraquinone-based anionic dye is carcinogenic and polluting to the environment. The anthraquinone dye is a resilient substance in the environment, making it challenging to treat these dyes using procedures that cause them to degrade in water [22, 24].

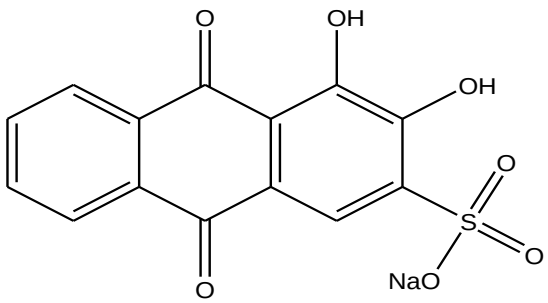

Figure 1. Chemical structure of ARS

ISSN (Online) 2456 -1304

International Journal of Science, Engineering and Management (IJSEM)

Vol 10, Issue 3, March 2023

II. EXPERIMENTAL

2.1. Materials and Method

We acquired Tetraethylorthosilicate (TEOS,≥98%), 3 aminopropyltriothoxysilane (APTES≥98%), CetylTrimethylAmmonium Bromide (CTAB,≥98%), and Alizarin Red S (ARS) from Sigma-Aldrich for the removal experiment as well as $FeCl_3.6H_2O$, $FeCl_2.4H_2O$, ethanol, and ammonia solution (25 percent) from Merck for the synthesis of the nanocomposite. The dye stock solution (1000 mg/L) was obtained by dissolving 0.05 gr of dye in 50 mL of double distilled water. Merck supplied us with HCl (37% concentration) and NaOH for pH adjustment.

2.2. Instrument

The morphology and particle size of the nanocomposite were investigated using a scanning electron microscope (SEM) model FE-SEM from TESCAN and a transmission electron microscope (TEM) model Zeiss-EM10C operating at an accelerated voltage of 80 kV. Fourier transform infrared (FT-IR) Shimadzu model 8400S was used to analyze the modification surface of the nanocomposite. The operating X-ray radiation from Panalytical Co. was used to characterize the magnetic core-shell nanocomposite using XRD patterns on the X' Pert Pro. Shimadzu model 1800 double beam UV-visible spectrophotometer was utilized to ascertain the adsorption dye changed upon absorption. The pH-meter model 3BW microprocessor was used to measure the impact of pH on adsorption and Software Design-Expert 10 trial was used to carry out the design experiment (Stat-Esae Inc.,MN,USA).

2.3. Synthesis core-shell Fe3O4@MCM-41-NH2

Prepare Fe_3O_4 as the core first using the co-precipitation method with a few modifications using the procedure already published [25]. The basis for this approach is a mixture of Fe^{+2} and Fe^{+3} in a molar ratio of 1:2, followed by the addition of 5 ml of 25% ammonia solution in atmosphere N_2 while the mixture is being violently stirred. After four hours, gather the product using an external magnetic field, wash three orders with double-distilled water, and then dry it in an oven at 50 °C. The following stage involves creating magnetic mesoporous using the Stöber method [26]. The chemical process used to create this nanocomposite involves dispersing 0.050 gr of dry nanomagnetic in a 1:2 volume mixture of ethanol and water. This mixture remained for around 30 minutes in an ultrasonic to achieve a homogenized mixture. After that, 1.2 ml of an ammonia solution was added to the solution and swirled for roughly an hour. The development of the MCM-41 structure on the nanomagnetic surface was accomplished by gently adding 0.364 gr of CTAB into 10 ml of double-distilled water to the magnetic solution. After stirring for an hour, 1.05 grams of TEOS were added dropwise, and the mixture was mixed at room temperature for 24 hours. As a result, the nanoparticle was cleaned with an ethanol/distilled water solution to get rid of any remaining CTAB on the surface before being dried at 40 °C in an oven. The final stage was to obtain the core-shell structure by calcining at 550 °C for 6 hours in an air environment.

2.3.1. Modified nanocomposite for applying to remove dye

Silanol groups on the surface of nanocomposite materials interact with APTES. The steps are as follows: 30 ml of anhydrous toluene, 3 ml of APTES, and 0.5 gr of the magnetic nanocomposite were added. This reaction took place in an environment of N_2 and refluxed for 12 hours at 60 °C. Following the amino-function on the core shell, the material was collected using an external magnet, washed with ethanol (3–5ml), and dried at 60 °C in the oven.

2.4. Design experimental and data analysis

In this study, central composite design (CCD) was used as the primary tool for optimizing the key parameters on maximum dye removal. To begin with, certain experiments were conducted to determine the parameter's level limitations. The key factors that affected dye removal were found to be pH, vortex time, absorbent quantity, and dye concentration.

2.5. Adsorption experimental MNPs based D-µ-SPE procedure

The initial experiment was carried out by adding 16 ppm of ARS to 25 ml of distilled water in a 50 ml beaker, followed by the addition of Fe3O4@MCM-41-NH2 and the adjustment of pH with 0.1 M HCl or 0.1 M NaOH. A vortex was used to stir the liquid for 4 minutes to help the adsorbent disperse. An external magnet was used to collect the magnetic adsorbent. Finally, using a magnet to separate the absorbed, the concentration of ARS that remained in the solution was determined using a UV-Visible spectrophotometer at maximum wavelengths. Schematic design of the proposed process is represented in scheme 1.

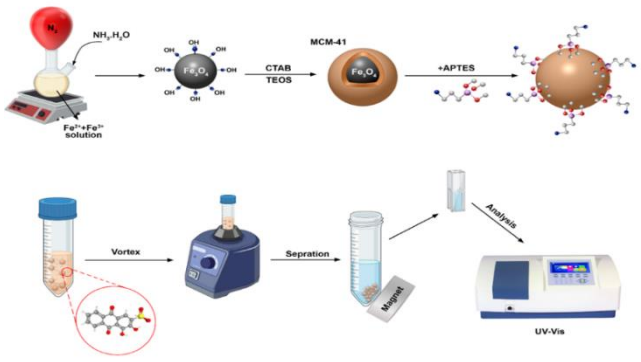

Scheme 1. Employed schematic experiment for the rapid removal of ARS from environmental wastewater samples using magnetic core-shell Fe_3O_4@MCM-41-NH_2 .

2.6. Proficiency absorbent

Desorption and reusability are the two key criteria for judging an absorbent's proficiency.The desorption

ISSN (Online) 2456 -1304

International Journal of Science, Engineering and Management (IJSEM)

Vol 10, Issue 3, March 2023

experiment was carried out separately with 25 ml of dye at 20 ppm. The absorbent was then collected and washed with 1 ml of various solvents such as Methanol, Ethanol, and Acetone, 10% HCl 0.1 molar, and 10% NaOH 0.1 molar. Then, the mixture was agitated for 4 minutes, and the concentration of magnetic nanoparticles and ARS remaining in the solvent were determined using a UV-Vis spectrophotometer. To test the absorbent's reusability, it was washed three times with 1 ml acetone to remove ARS that had become adsorbed on the surface of the absorbent, then washed with Ethanol/water 50:50 and dried in an oven at 40 °C.

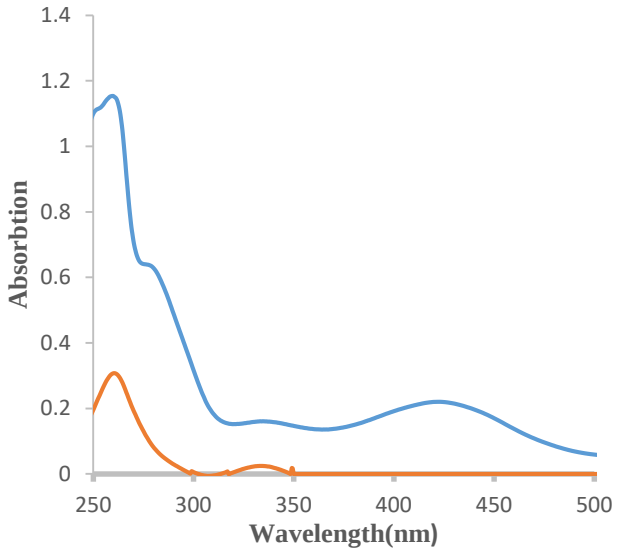

Figure 2. Removal 16 mg.L^{-1} ARS by 0.007gr NMM at pH 3 about 3 min

III. RESULT AND DISCUSSION

3.1. Characterization of Fe3O4@MCM-41-NH2

SEM was used to investigate the morphology , chemical composition of the sample. The shape and size of nanoporous were determined by TEM, as illustrated in Fig. 3.

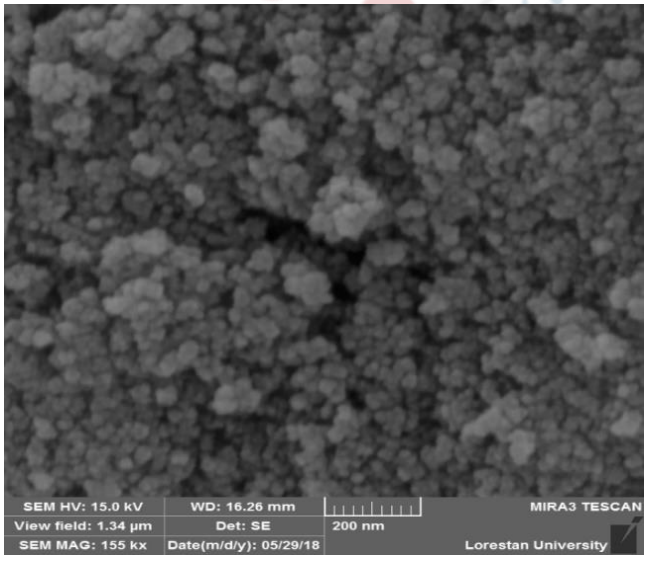

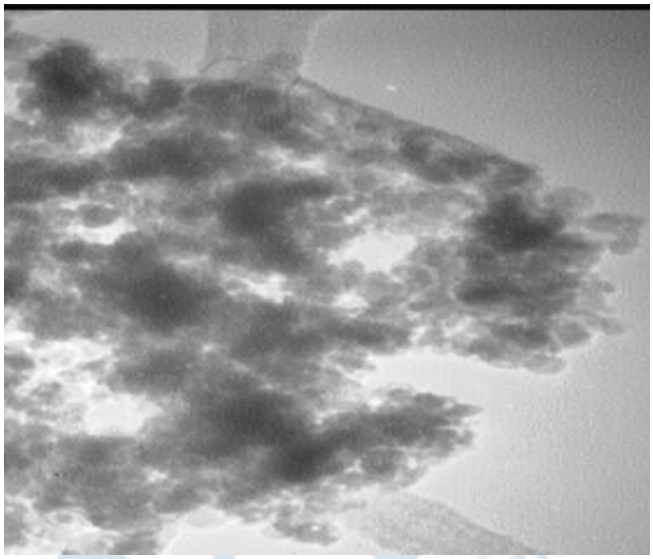

Figure 3. Images SEM and TEM of Fe_3O_4@MCM-41-NH_2

A spherical particle with a mesoporous shell immobilized on the surface and a dark-colored Fe_3O_4 core can be seen in the TEM pictures of Fe_3O_4@MCM-41-NH2.

The FT-IR spectra at 400-4000 cm^{-1} range show the modification surface with APTES in Fig.4.

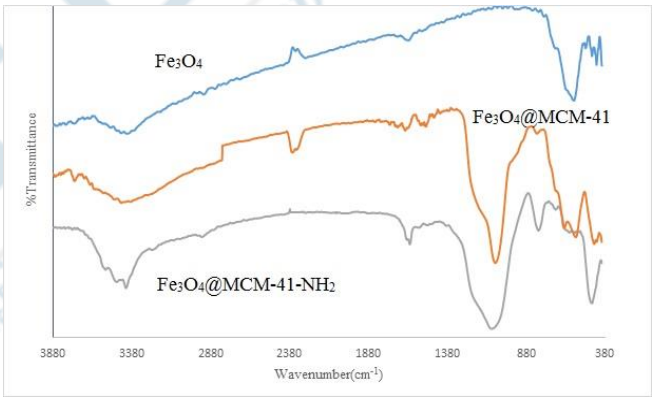

Figure 4.FT-IR spectra of synthesis nanopartilces

In FT-IR spectroscopy of Fe_3O_4, Fe_3O_4@MCM-41, and Fe_3O_4 modified with APTES, the stretching vibration O-H was identified at 3380 cm^{-1} and a peak corresponding to Fe-O at roughly 580 cm^{-1} could be found [27]. The FT-IR indicated the presence of a mesoporous shell on a surface nano magnet because three peaks were detected: 1080 cm^{-1}, 807 cm^{-1}, and 459 cm^{-1} for Fe_3O_4@MCM-41, which were attributed to stretching of Si-O, and a peak at 790 cm^{-1} for bending vibration of Si-OH in mesoporous [28]. Figure 5 shows two distinct bands at 2931 and 1618cm^{-1} that corresponds to the -CH_2 stretching and bending vibrations of the bond N-H, respectively.

We used X-ray diffractograms to characterize the Fe3O4 nanomagnetic and Fe_3O_4@MCM-41-NH_2 core-shell nanocomposite as shown in Fig.5.

ISSN (Online) 2456 -1304

International Journal of Science, Engineering and Management (IJSEM)

Vol 10, Issue 3, March 2023

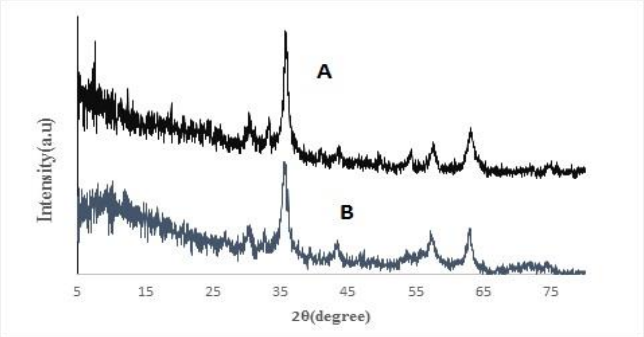

Figure 5.XRD pattern A)Fe_3O_4 B) Fe_3O_4@MCM-41-NH_2

The nanomagnetic in the pattern XRD has six peaks at 30.1, 35.5, 43.1, 53.4, 57.0, and 62.6 with 2 peaks linked to magnetic nanoporous as identical to nanomagnetic, which showed that Fe_3O_4 nanomagnetic as core. There are no peaks visible connected to nanomesoporous because silica is structure amorphous.

3.2. Optimization

Different parameters, such as ionic strength, pH, amount of absorbent, dye concentration, and type of solvent desorption, have an impact on dye removal and must be optimized to achieve maximal removal.

To reduce the number of experiments in CCD, we first determined the parameters that affect dye removal. The ionic strength parameter was examined using NaCl in the range of (0-5 percent w/v) in 25 ml of solution with 20 ppm of dye. The outcome is presented in Fig.6.

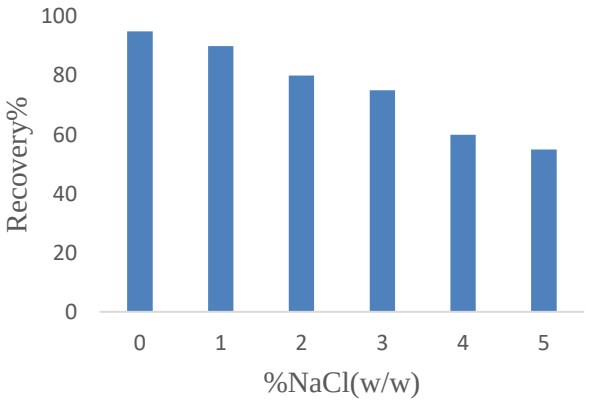

Figure 6. Effect of adding salt for removal ARS

The removal dye was reduced as the ionic strength increased. The two primary causes of this observation have been identified. First, higher Cl^- adsorption on the surface absorbent in comparison to anionic dye; second, adding salt reduces the diffusion film that rate of anionic transfer from the bulk solution to on-surface modified nanomagnetic MCM-41. So, the study was performed without any salt [29].

Other parameters including pH, absorbent quantity, vortex time, and dye concentration were analyzed by CCD and are reported in Table 1.

Table.1. CCD reports with analysis.

Table.1. Main factors that effectively on removal and levels coded for CCD

		Level			
Variables	unite	Low	High	-α	+α
pH(A)	-	3.5	6.5	2	8
M adsorbent(B)	gr	0.0075	0.0125	0.005	0.015
vortex time (C)	min	2	4	1	5
ARS Concentration(D)	ppm	9	19	4	24

Four independent factors and four levels of the central composite design for dye removal. We have four independent components at two levels that were designed for 30 experiments in one block in the CCD. Following design, we conduct experiments and compute dye recovery. The results are displayed in Table 2.

Table 2. Central composite design for ARS

Run	A	B	C	D	R%	Run	A	B	C	D	R (ARS) %
1	5	0.015	14	3	89.63	16	6.5	0.0075	19	4	78.22
2	5	0.01	14	3	78.42	17	5	0.01	14	3	74.56
3	3.5	0.0075	9	2	71.79	18	5	0.01	24	3	67.78
4	3.5	0.0075	9	4	74.2	19	6.5	0.0075	9	4	78.56
5	6.5	0.0125	19	2	94.4	20	5	0.01	14	3	66.81
6	3.5	0.0125	9	2	79.59	21	6.5	0.0075	9	2	78.42
7	5	0.01	4	3	22.78	22	5	0.01	14	3	92.37
8	5	0.01	14	3	95.49	23	3.5	0.0125	19	4	78.24
9	3.5	0.0125	9	4	63.68	24	5	0.01	14	3	76.71
10	8	0.01	14	3	82.93	25	6.5	0.0125	19	4	81.55
11	5	0.01	14	5	76.5	26	5	0.01	14	1	75.87
12	6.5	0.0125	9	2	63.98	27	3.5	0.0075	19	4	62.61
13	5	0.005	14	3	65.35	28	3.5	0.0125	19	2	79.3
14	6.5	0.0075	19	2	80.09	29	3.5	0.0075	19	2	93.65
15	6.5	0.0125	9	4	65.14	30	2	0.01	14	3	78.22

The analytical response for dye removal was performed, and the results showed that the quadratic equation was the optimum model to evaluate dye response. This equation is as follows:

$$Y=b_0+\sum_{i=1}^{n} b_i x_i+\sum_{i=1}^{n} b_{ii} x_i^2+\sum_{i=1}^{n}\sum_{j=i+1}^{n} b_{ij} x_i x_j \quad (1)$$

In this equation, Y is the dependent variable, which is the percentage recovery, b_0 is the constant model, x_i is the independent variables, bi is the coefficient for the linear model, b_{ii} is the coefficient for the quadratic model, and b_{ij} is the interaction coefficients between the independent variables.Using the Analysis Variance (ANOVA) to investigate the model and the result are shown in Table. 3

ISSN (Online) 2456 -1304

International Journal of Science, Engineering and Management (IJSEM)

Vol 10, Issue 3, March 2023

Table.3.Analysis variance(ANOVA) for removal ARS

	Sum of Squares	df	Mean Square	F Value	p-value	
Model	2406.73	14	171.91	1413.59	< 0.0001	S
A-pH	1323.58	1	1323.58	10883.62	< 0.0001	
B-Madsorb	970.15	1	970.15	7977.45	< 0.0001	
C- ARS	38.43	1	38.43	316.01	< 0.0001	
D-time	1.32	1	1.32	10.86	0.0049	
AB	16.91	1	16.91	139.07	< 0.0001	
AC	0.039	1	0.039	0.32	0.5795	
AD	7.36	1	7.36	60.5	< 0.0001	
BC	0.043	1	0.043	0.35	0.5607	
BD	7.6	1	7.6	62.53	< 0.0001	
CD	1.97	1	1.97	16.17	0.0011	
A^2	0.54	1	0.54	4.46	0.0518	
B^2	2.89	1	2.89	23.73	0.0002	
C^2	1.88	1	1.88	15.46	0.0013	
D^2	29.35	1	29.35	241.32	< 0.0001	
Residual	1.82	15	0.12			
Lack of Fit	1.12	10	0.11	0.8	0.6465	N.S
Pure Error	0.7	5	0.14			
Cor Total	2408.56	29				

We constructed an equation that explains the maximum removal of dye. The equation is as follows:

Maximum removal of ARS (%) =78.29-7.43*A+6.36*B-1.27*C+0.23*D-1.03*AB+0.049*AC+0.68*AD-0.052*BC+0.69*BD-0.35*CD+0.14*A^2-0.32*B^2

ANOVA was used in the experiment. Some parameters are critical: One is the model significance (F value 1413.59), and another is Lack of Fit (LOF) of 0.6465.

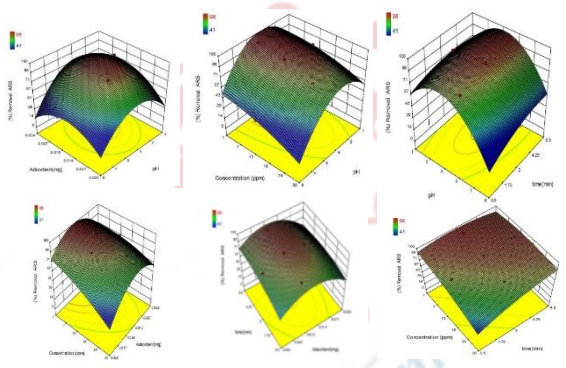

Figure 7. 3D plots for removal ARS

Using a 3D graphic, the impact of independent variables on the response was examined

The study of the influence of pH removal is an effective parameter on adsorption and dye removal because it changes the media of solution and the location of on-surface adsorbent that produces adsorbent dye. As electrostatic interaction between positive surface nano particle and negative dye was observed, we can conclude that maximum removal occurs under acidic conditions [30]. Analysing the effect of sorbent on removal over the range of 0.005-0.0115 gr revealed that as sorbent concentration increased, dye removal also increased. This increase in removal is due to the availability of a large surface area. The results showed that increasing the vortex time to 5 minutes increased ARS dye clearance. This adsorption is caused by a large surface area and a short diffusional channel. In comparison to other adsorbents, the time equilibrium inside the adsorbent and solution in this experiment is relatively brief.

The relationship between the initial concentration of dye and removal percentage was examined, and the results show that as the initial concentration of dye increases, the removal percentage decreases. This behaviour is related to an increase in the initial concentration dye to surface area ratio, which causes less mass transfer.

The results of the research revealed that the optimal condition for removal was a pH of 3.5, a quantity of adsorbent of 0.013, and a vortex period of 4 minutes for ARS. Under these conditions, we can remove 95.65% of the ARS from aqueous solutions.

3.3. Studying absorption kinetics

Understanding the adsorption process of this nanomagnetic, such as chemical reaction, diffusion control, and mass transport was obtained by investigating the adsorption isotherm [31].

This experiment was carried out separately for both dyes in 25 ml solutions of 16 ppm each dye with 0.007 of adsorbent that vortex for an approximately adequate duration and determined dye removal by Eq.(2):

$$\text{Percentage removal dye (\%)} = \frac{C_0 - C_r}{C_0} \times 100 \quad (2)$$

In this equation, C_0 is the initial concentration (ppm) and C_r is the concentration dye (ppm) after removal.

To achieve equilibrium data, kinetic models of pseudo-first [32] and second order[33], inter-particle diffusion[34] as well as The Elovich equation [35], were examined. The equation to calculate psedu-first order is:

$$\ln(q_e - q_t) = \ln q_e - K_1 t \quad (3)$$

where q_e (mg/g), q_t (mg/g), and K_1 (psdeuo first-order constant) are the amounts of dye that nanomagnetic absorb at equilibrium and time t (min^{-1}), respectively (min^{-1}). The amount of dye absorbed by the adsorbent in psdeu second-order depends on the number of surface-active sites. The equation for second-order psdeuo is given as:

$$\frac{t}{Q_t} = \frac{1}{K_2 Q^2_e} + \frac{t}{Q_e} \quad (4)$$

In this equation, K_2 is constant pseduo second-order ($gmg^{-1}min^{-1}$).

First, the dye was adsorbed on the surface in a nanomagnetic manner, and then the absorption was managed via micro-intraparticle diffusion. the equation for inter-particle diffusion is;

$$Q_t = K_p t^{0.5} + C \quad (5)$$

ISSN (Online) 2456 -1304

International Journal of Science, Engineering and Management (IJSEM)

Vol 10, Issue 3, March 2023

In this equation, K_p(mg(g $min^{1/2})^{-1}$) is constant interaparticle diffusion and C is the boundary layer thickness.

The Elovich equation, which has the following linear form, can also be used to examine the adsorption data:

$q_t = \beta \ln(\alpha\beta) + \beta \ln t$ (6)

Table 4 displays the findings. We can conclude that pseudo-second order is the best fit model for data experiments since it was chosen as the best model based on a high-value linear correlation coefficient, r^2.

Table.4. Kinetic parameters for ARS

Model	parameters	Concentration ARS		
		10	15	20
First order kinetic	$k_1(min^{-1})$	0.2982	0.4675	0.8656
	$q_e calc((mg.g^{-1})$	33.13	65.72	81.71
	R^2	0.9019	0.946	0.8115
Pesudeo-second-order kinetic	$k_2(min^{-1})$	0.0055	0.0029	0.0012
	$q_e(calc((mg.g^{-1)})$	75.14	81.43	90.35
	R^2	0.9909	0.9916	0.9978
Intrapartcle diffusion	$K_{diff}(mg.g^{-1}.min^{-1.2})$	26.13	32.18	34.62
	C $(mg.g^{-1})$	18.49	16.58	31.93
	R^2	0.9836	0.9516	0.9039
Elovich	B	0.095	0.066	0.138
	A	93.5	85.97	80.1
	R^2	0.9629	0.9467	0.80

3.4. Studying isotherm adsorption

Using the Langmuir, Freundlich, Dubinin, and Radushkevich (D-R), and Timken isotherm models, the equilibrium isotherm of an adsorbent for the removal of ARS ions at ambient temperature was investigated. The Langmuir isotherm model predicts monolayer coverage of ARS ions on the adsorbent's outer surface. The Langmuir isotherm can be presented in linear form as follows:

The Langmuir equation is:

$C_e/Q_e = 1/(K_L Q_{max}) + (1/Q_{max}) C_e$ (7)

Where Qe (mg.g-1) indicates the equilibrium solute adsorption amount, Ce $(mg.L^{-1})$ indicates the equilibrium solute concentration, Qm indicates the maximum monolayer adsorbent ion capacity $(mg.g^{-1})$, and $K_L(L.mg^{-1})$ indicates the Langmuir constant. Regarding this equation, the C_e/Q_e has a linear correlation with C_e.

$q_e = q_m b C_e/(1+bC_e)$ (8)

A plot of $1/q_e$ versus $1/C_e$ should indicate a line with slope b(the Langmuir adsorption constant$(L.mg^{-1})$) and intercept of q_m (theoretical maximum adsorption capacity$(mg\ g^{-1})$) [36].

Another model that represents the surface with adsorption heterogeneity is the Freundlich empirical equation model. The Freundlich isotherm's linear form is as follows:

$$Ln(q_e) = LnK_F + \frac{1}{n} LnC_e \quad (9)$$

K_F and n are Freundlich constants that represent the capacity and intensity of adsorption, respectively. The slope and intercept of a linear plot of lnq_e versus lnC_e were used to estimate the values of Kf and n, respectively [37].

The Timken model provides details on the heat of adsorption and the interaction between the adsorbent and adsorbate. The Temkin isotherm linear equation is as follows:

$q_e = B \ln K_T + B \ln C_e$ (10)

The Temkin constant is B $(j.mol^{-1})$ and the equilibrium binding constant is K_T $(L.mol^{-1})$.

The Dobinin-Rodushkvich isotherm is used to determine the mean free energy of adsorption (β), which is related to the chemical and physical properties of adsorption [38].

The linear version of the D-R isotherm is represented as follows:

$lnq_e = lnq_s - \beta R^2 T^2 Ln(1+1/C)^2$ (11)

Adsorption energy $(\beta mol^2(Kj^2)^{-1})$ and theoretical saturation capacity were calculated in this model using the slope and intercept of the linear plot lnqe vs. $Ln(1+1/C))^2$ [39].

ISSN (Online) 2456 -1304

International Journal of Science, Engineering and Management (IJSEM)

Vol 10, Issue 3, March 2023

Table.5. Parameter isotherms for ARS

Isotherm	Parameters	Value of parameter	Isotherm	Parameters	Value of parameter
Longmuir	$q_m(mg.g^{-1})$	192.27	Temkin	$K_T(L.mg^{-1})$	0.51
	$K_L(L.mg^{-1})$	0.0553		B_1	92.59
	R^2	0.9995		R^2	0.9056
Freundlich	n/1	1.49	D-R	$q_s(mg.g^{-1})$	3812.17
				E	9498.05
	$K_F(L.mg^{-1})$	14.1		$B\times10^{-9}$	6.12
	R^2	0.9523		R^2	0.9912

Table 5 shows the results of fitting the experimental data in isotherm models, as well as the values of the parameters and their corresponding correlation coefficients. The Freundlich isotherm with the greatest correlation coefficient (R^2) value can be utilized to describe ARS ion adsorption on magnetic nonporous.

IV. COMPARESSON THIS METHOD REMOVAL ARS DYE WITH OTHER METHODS

Table 6 compares this method of colour removal with other ways of dye removal. In comparison to other approaches, the results demonstrated the effectiveness of this procedure for removing ARS.

Table.6. Compariation this method removal with other methods

Adsorbent	time(min)	$q_m(mgg^{-1})$	Ref.
MAC	300	108.69	[40]
Fe3O4	25	45.87	[41]
Fe_3O_4@NiO	90	223.3	[42]
Pentaerythritol-modifed carbon nanotube	30	257.73	[43]
Fe_3O_4@MCM-41-NH_2	10	224.21	This work

V. CONCLUSION

In this study, we used nanomagnetic adsorption, which is an efficient, quick, and low-cost method of removing anionic dye. The removal was affected by several parameters, including pH, adsorption quantity, and time vortex. Based on the findings, the highest rate of dye removal was achieved at pH sample 3.5, 0.013gr absorbent, 4 min of vortex time, and 9 mg/l of ARS Concentration .This rate of dye removal efficiency was 95.65 percent This factor was optimized for maximal removal by CCD, and the results showed that modified magnetic Nano porous is a good absorbent for anionic dye removal from aqueous solutions. The model's kinetics were investigated, and the results indicated that the pseudo-second order model fits the data the best. The Langmuir model was fitted to the dye and equilibrium data, confirming that a monolayer of dye forms on the surface of the adsorbent. The further results indicated that we can extract 95.65 percent ARS from an aqueous solution. This approach has an advantage over other methods of removing anionic dye since it has a high absorption capacity of 224.21 for ARS and uses a small amount of sorbent (0.013g) for a short period of (4 min).

VI. ACKNOWLEDGMENTS

The authors want to thank the authorities of *Komar University of Science and Technology* for their support from this study.

REFERENCES

[1] M. F. Hanafi and N. Sapawe, Materials Today: Proceedings **31**, A141-A150 (2020).
[2] K. G. Pavithra and V. Jaikumar, Journal of Industrial and Engineering Chemistry **75**, 1-19 (2019).
[3] A. B. Dos Santos, F. Cervantes, R. Yaya-Beas and J. Van Lier, Enzyme and Microbial Technology **33** (7), 942-951 (2003).
[4] D. Brown, Ecotoxicology and environmental safety **13** (2), 139-147 (1987).
[5] C. A. Fewson, Trends in biotechnology **6** (7), 148-153 (1988).
[6] Y. Fu and T. Viraraghavan, Bioresource technology **79** (3), 251-262 (2001).
[7] R. B. Narayan, R. Goutham, B. Srikanth and K. Gopinath, Journal of environmental chemical engineering **6** (3), 3640-3647 (2018).
[8] Y. Zhu and P. Kolar, Journal of Environmental Chemical Engineering **2** (4), 2050-2058 (2014).
[9] S. Wang and H. Wu, Journal of hazardous materials **136** (3), 482-501 (2006).
[10] Y. Huang, J. Li, X. Chen and X. Wang, RSC Advances **4** (107), 62160-62178 (2014).
[11] Y. Yang, J. Ma, Q. Qin and X. Zhai, Journal of Molecular Catalysis A: Chemical **267** (1), 41-48 (2007).
[12] D. Shao, G. Hou, J. Li, T. Wen, X. Ren and X. Wang, Chemical Engineering Journal **255**, 604-612 (2014).
[13] S. Zhang, M. Zeng, W. Xu, J. Li, J. Li, J. Xu and X. Wang, Dalton Transactions **42** (22), 7854-7858 (2013).
[14] M. Faraji, Y. Yamini and M. Rezaee, Journal of the Iranian Chemical Society **7** (1), 1-37 (2010).
[15] J. Li, Z. Guo, S. Zhang and X. Wang, Chemical engineering

journal **172** (2), 892-897 (2011).
[16] B. Zargar, H. Parham and A. Hatamie, Talanta **77** (4), 1328-1331 (2009).
[17] J. M. Rosenholm, J. Zhang, W. Sun and H. Gu, Microporous and Mesoporous Materials **145** (1), 14-20 (2011).
[18] H. Yang, G. Li and Z. Ma, Journal of Materials Chemistry **22** (14), 6639-6648 (2012).
[19] Y. Chen and S. Mu, Sensors and Actuators B: Chemical **192**, 275-282 (2014).
[20] I. D. Mall, V. C. Srivastava, N. K. Agarwal and I. M. Mishra, Chemosphere **61** (4), 492-501 (2005).
[21] S. Parra, S. E. Stanca, I. Guasaquillo and K. R. Thampi, Applied Catalysis B: Environmental **51** (2), 107-116 (2004).
[22] M. Ghaedi, A. Hassanzadeh and S. N. Kokhdan, Journal of Chemical & Engineering Data **56** (5), 2511-2520 (2011).
[23] T. Moriguchi, K. Yano, S. Nakagawa and F. Kaji, Journal of colloid and interface science **260** (1), 19-25 (2003).
[24] S. Chatterjee, S. Chatterjee, B. P. Chatterjee and A. K. Guha, Colloids and Surfaces A: Physicochemical and Engineering Aspects **299** (1), 146-152 (2007).
[25] E. Khaledyan, K. Alizadeh and Y. Mansourpanah, Iranian Journal of Science and Technology, Transactions A: Science **43** (3), 801-811 (2019).
[26] W. Stöber, A. Fink and E. Bohn, Journal of colloid and interface science **26** (1), 62-69 (1968).
[27] J. Lee, T. Isobe and M. Senna, Journal of Colloid and Interface Science **177** (2), 490-494 (1996).
[28] A. Khorshidi and S. Shariati, RSC Advances **4** (78), 41469-41475 (2014).
[29] M. B. Gholivand, Y. Yamini, M. Dayeni, S. Seidi and E. Tahmasebi, Journal of Environmental Chemical Engineering **3** (1), 529-540 (2015).
[30] Y. Wu, M. Zhang, H. Zhao, S. Yang and A. Arkin, RSC Advances **4** (106), 61256-61267 (2014).
[31] A. Joglekar and A. May, Cereal foods world **32** (12), 857-& (1987).
[32] A. B. Albadarin, C. Mangwandi, H. Ala'a, G. M. Walker, S. J. Allen and M. N. Ahmad, Chemical Engineering Journal **179**, 193-202 (2012).
[33] L. Shi, D. Wei, H. H. Ngo, W. Guo, B. Du and Q. Wei, Bioresource technology **194**, 297-304 (2015).
[34] Y.-S. Ho and G. McKay, Process Safety and Environmental Protection **76** (2), 183-191 (1998).
[35] M. Ghaedi, A. Ghaedi, E. Negintaji, A. Ansari, A. Vafaei and M. Rajabi, Journal of Industrial and Engineering Chemistry **20** (4), 1793-1803 (2014).
[36] I. Langmuir, Journal of the American chemical society **38** (11), 2221-2295 (1916).
[37] W. J. Weber and J. C. Morris, Journal of the Sanitary Engineering Division **89** (2), 31-60 (1963).
[38] M. Ghaedi, A. Ansari, M. Habibi and A. Asghari, Journal of Industrial and Engineering Chemistry **20** (1), 17-28 (2014).
[39] M. Dubinin and V. Serpinsky, Carbon **19** (5), 402-403 (1981).
[40] M. Fayazi, M. Ghanei-Motlagh and M. A. Taher, Materials Science in Semiconductor Processing **40**, 35-43 (2015).
[41] G. Absalan, A. Bananejad and M. Ghaemi, Analytical and Bioanalytical Chemistry Research **4** (1), 65-77 (2017).
[42] R. Nodehi, H. Shayesteh and A. Rahbar-Kelishami, International Journal of Environmental Science and Technology **19** (4), 2899-2912 (2022).
[43] J.-Y. Yang, X.-Y. Jiang, F.-P. Jiao and J.-G. Yu, Applied Surface Science **436**, 198-206 (2018).